INTERACTION OF NIOBIUM WITH POLYCRYSTALLINE PALLADIUM SURFACE. X-RAY PHOTOEMISSION STUDY

Ivan JIRKA[1,*] and Zdeněk BASTL[2]

J. Heyrovský Institute of Physical Chemistry, Academy of Sciences of the Czech Republic, v.v.i., Dolejškova 3, 182 23 Prague 8, Czech Republic; e-mail: [1] ivan.jirka@jh-inst.cas.cz, [2] zdenek.bastl@jh-inst.cas.cz

Received May 13, 2008
Accepted August 18, 2008
Published online November 27, 2008

Dedicated to Professor Rudolf Zahradník on the occasion of his 80th birthday.

Evolution of niobium–palladium (Nb–Pd) interface alloy prepared by *in situ* Nb deposition on highly defect polycrystalline Pd surface at room temperature has been investigated using X-ray photoelectron spectroscopy. The binding energies of the Nb $3d_{5/2}$ and Pd $3d_{5/2}$ core-level lines and their line shapes and the kinetic energies and shapes of Pd $M_{4,5}N_{4,5}N_{4,5}$ Auger spectrum have been used to characterize the Nb–Pd system. A two-step growth mode of the Nb adlayer has been observed: a two-dimensional (2D)-like growth in a submonolayer Nb concentration region and three-dimensional (3D) intermixing of Nb and Pd atoms at Nb loadings above the monolayer coverage. The latter growth mode resulted in appearance of rather homogeneous Nb–Pd alloy phase.

Keywords: Auger spectrum; X-ray photoelectron spectroscopy; Polycrystalline surfaces; Monolayers; Nb–Pd surface alloy; Nb growth mode; XPS.

Alloys of palladium with some other metal are extensively investigated as membrane hydrogen separators[1] and membrane catalysts for variety of hydrogenation reactions[2]. Addition of another metal can help to improve mechanical properties of Pd membrane and can enhance its permeability. Variety of metals introduced into Pd membrane, like silver, titanium, nickel, copper and ruthenium were already tested from this point of view. The Nb–Pd alloy with high niobium content was found to obey better mechanical and hydrogen permeation properties than the most often used Pd–Ag alloy[3]. To get inside into the role of Nb addition in the membrane a model system prepared by vacuum deposition of Nb on highly defect polycrystalline surface of Pd is investigated in the present study. Alloying at various stages of Nb deposition is studied by X-ray photoelectron spectros-

Collect. Czech. Chem. Commun. 2008, Vol. 73, No. 10, pp. 1314–1326

doi:10.1135/cccc20081314

copy (XPS). This study is a continuation of our previous work[4] where Pd deposited on Nb polycrystalline surface was studied and appearance at room temperature of a Pd–Nb alloy-like surface phase in the region of submonolayer coverage was demonstrated. The thermal stability of Pd–Nb surface layer was investigated.

A variety of electronic effects appear in bimetallic bonding of Pd with various electropositive metals. The charge transfer effects and the rehybridization of the Pd valence levels were most frequently discussed[5–8]. These effects induce core level binding energy shifts of both the Pd and adlayer metal to energies of higher values relative to those of pure metals, upon appearance of bimetallic bonds.

The chemical bonding between Pd adatoms and various Nb monocrystalline surfaces was already proved[9,10]. The Pd–Nb surface alloy was observed for submonolayer Pd coverages. The Pd–Nb intermixing was observed above a monolayer coverage upon annealing. However, according to our best knowledge the interaction of Nb adlayer with Pd has not yet been experimentally investigated.

The aim of present study is to get inside the nature of interaction of Nb adatoms with Pd support below and above a monolayer Nb coverage. Obtained information is valuable for understanding of the chemical properties of real Nb–Pd bimetallic catalyst prepared by physical vapor deposition. Polycrystalline Pd with highly defect surface was thus selected as a support. The investigation is based on discussion of Nb 3d and Pd 3d line intensities, shapes and binding energies, and kinetic energies of the electrons emitted by Auger Pd MNN transition in dependence on the deposited amount of Nb. Additional experiments with Pd deposits on a Nb surface were carried out in this study for the sake of comparison. The latter system is referred to below as Pd/Nb.

EXPERIMENTAL

The experiments were performed using an ESCA III Mk 2 (VG Scientific) photoelectron spectrometer equipped with an AlKα X-ray source and hemispherical electron analyzer. The pressure of residual gases during the experiments was below ~10^{-8} Pa. High purity Pd and Nb foils (99.99%) were used as the substrates. The Pd and Nb surfaces were cleaned by argon ion sputtering (E = 6 kV, I = 40 μA) before deposition. The carbon–palladium (C/Pd) atomic ratio of sputtered Pd surface estimated from intensities of C 1s and Pd 3d photoelectron lines was ~10^{-2}. No oxygen contamination was observed. Nb was then evaporated from a thin filament with rate of 7.6 × 10^{12} atoms Nb cm^{-2} s^{-1}. Pd was evaporated from a tungsten filament using a liquid nitrogen cooled evaporator at the evaporation rate 4.2 × 10^{12} atoms Pd cm^{-2} s^{-1}. The rate of Nb (Pd) evaporation was estimated by plotting the calculated Nb concentration (in submonolayer concentration region) against deposition time t (for $t \leq$

240 s). Desirability of this procedure is discussed below. Data from our previous study[4] were used for estimation of Pd evaporation rate. The evaporation rates were reproducible within 5%. The base pressure during evaporation was better then ~10^{-8} Pa. About two-fold increase of C/Pd atomic ratio was observed upon Nb evaporation, however, no evidence was found for the presence of oxygen contamination. The photoelectron and Auger spectra were measured at high resolution in order Nb 3d, Pd 3d and Pd $M_{4,5}N_{4,5}N_{4,5}$. The photoelectron spectra were simulated by a damped non-linear least square fitting procedure using asymmetrical pseudo-Voight functions. Prior to fitting the Shirley background was subtracted.

To estimate the evaporation rate of Nb the surface concentration c_s of Nb deposits was calculated from the thickness of Nb adlayer assuming two-dimensional (2D) growth mode of Nb. The values of d were calculated by the following equation[11]:

$$\frac{I(\mathrm{Nb\,3d})}{I(\mathrm{Pd\,3d})} = \frac{I(\mathrm{Nb\,3d})_0}{I(\mathrm{Pd\,3d})_0} \frac{1 - \mathrm{e}^{-\frac{d}{\lambda(\mathrm{Nb\,3d})\sin\Theta}}}{\mathrm{e}^{-\frac{d}{\lambda(\mathrm{Pd\,3d})\sin\Theta}}} \qquad (1)$$

where I(Nb 3d)/I(Pd 3d) is the measured intensity ratio of the Nb 3d and Pd 3d photoelectron lines, d is the thickness of the Nb overlayer (in nm), λ(Pd 3d) and λ(Nb 3d) are the values of the inelastic mean free path of the photoelectrons emitted from the Pd 3d and Nb 3d levels (in nm), Θ is the detection angle (45°) with respect to the sample surface, and $I(\mathrm{Nb\,3d})_0$ and $I(\mathrm{Pd\,3d})_0$ are the photoelectron line intensities of pure Nb and Pd metal. The values of λ(Pd 3d) and λ(Nb 3d) are estimated using TPP-2M formula[12] (λ(Pd 3d) = 2.0 nm, λ(Nb 3d) = 2.7 nm). The $I(\mathrm{Nb\,3d})_0/I(\mathrm{Pd\,3d})_0$ intensity ratio was calculated from the following equation:

$$\frac{I(\mathrm{Nb\,3d})_0}{I(\mathrm{Pd\,3d})_0} = \frac{\sigma(\mathrm{Nb\,3d})\,\rho(\mathrm{Nb})\,M(\mathrm{Pd})\,T(\mathrm{Nb\,3d})\,\lambda(\mathrm{Nb\,3d})}{\sigma(\mathrm{Pd\,3d})\,\rho(\mathrm{Pd})\,M(\mathrm{Nb})\,T(\mathrm{Pd\,3d})\,\lambda(\mathrm{Pd\,3d})}\,. \qquad (2)$$

σ(Nb 3d (Pd 3d)), ρ(Nb (Pd)), M(Nb (Pd)), T(Nb 3d (Pd 3d)) and λ(Nb 3d (Pd 3d)) in Eq. (*2*) are the pertinent values of photoionization cross section[13], densities of Nb (Pd) (ρ(Nb) = 8.57 g cm^{-3}, ρ(Pd) = 12.00 g cm^{-3})[14] and transmission function of the analyzer ($T \sim E^{-1}$). The surface concentration of Nb, c_s (in atoms cm^{-2}) is related to d as follows:

$$c_s = \frac{\rho(\mathrm{Nb})}{M(\mathrm{Nb})}\, N_A\, d \times 10^{-7} \qquad (3)$$

where N_A is Avogadro constant. Analogous equations were used to calculate the surface concentration of Pd. The values of c_s thus obtained are expressed as the fraction of monolayer (1 ML Nb = 1.47 × 10^{15} atoms Nb cm^{-2}, 1 ML Pd = 1.67 × 10^{15} atoms Pd cm^{-2}, as calculated from bulk densities of Nb and Pd). The exactness of thus estimated surface concentration is limited mainly by desirability of used model of the adlayer growth mode (see below).

RESULTS

The measured intensities of Nb 3d and Pd 3d photoelectron lines plotted against the deposition time, t (bottom axis) and the corresponding surface concentration, c_s of Nb (top axis) are shown in Fig. 1. The intensity of the Pd 3d line was found to be independent within experimental error of the deposition time up to t = 240 s whereup it started to decrease; on the other hand, the intensity of the Nb 3d line increased linearly with t. The surface concentration of Nb at this deposition time as calculated by Eqs (*1*)–(*3*) is approximately equal to 1.2 ML Nb. A further linear increase of the intensity of the Nb 3d line above this deposition time (up to t = 900 s) with lower slope was obsereved. The two depositions of Pd on Nb (0.8 and 5.4 ML Pd) were also prepared.

The Nb 3d photoelectron spectra were simulated by one doublet with an optimized asymmetry and a spin orbital splitting of Δ = 2.75 eV (Fig. 2). The value of Δ employed was obtained by optimization of the Nb 3d spectrum of a clean Nb surface and was found to agree within experimental error with the value reported in literature[15] (Δ = 2.74 ± 0.09 eV). The binding

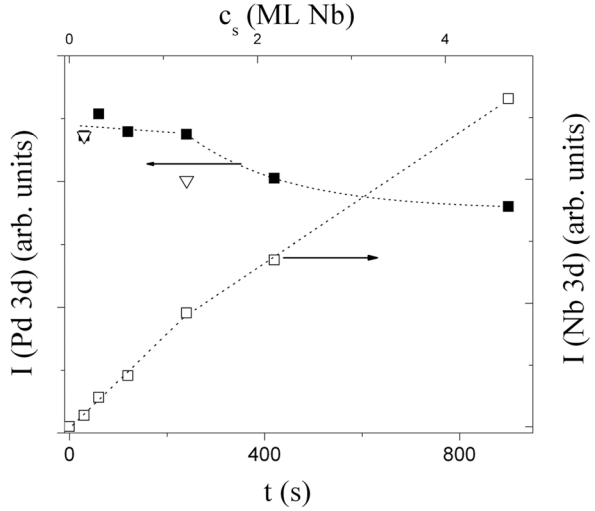

FIG. 1
Dependence of Nb 3d (□) and Pd 3d (■) photoelectron line intensities on evaporation time t (s) of Nb (bottom axis) and on Nb surface concentration c_s (ML Nb) (top axis). Calculated attenuation of Pd 3d intensity by ~0.1 and 1 monolayer of Nb (▽)

energy of the Nb $3d_{5/2}$ photoelectron line decreased from 204.3 eV for c_s ~ 0.1 ML Nb to 203.45 eV at the highest Nb loading (4.7 ML Nb) (see Fig. 3, Table I). The latter value is consistent with the value of the high energy Nb $3d_{5/2}$ photoelectron line in the Pd/Nb system (203.5 ± 0.2 eV).

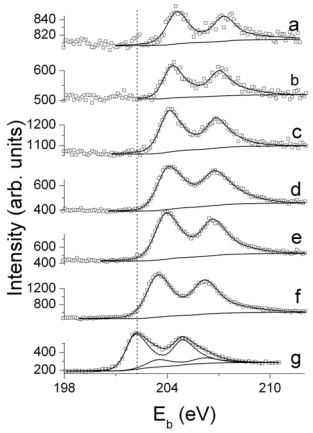

FIG. 2
Fitted Nb 3d spectra measured for the samples prepared using Nb deposits corresponding to 0.1 (a), 0.3 (b), 0.6 (c), 1.2 (d), 2.2 (e) and 4.7 (f) ML Nb, respectively, and the spectrum of the Pd–Nb sample containing 4.4 ML Pd (g)

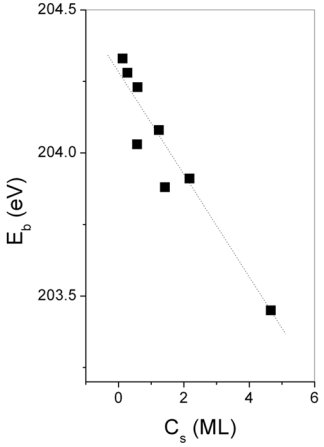

FIG. 3
Dependence of the Nb $3d_{5/2}$ core level binding energy E_b (eV) on surface concentration c_s (ML Nb)

The E_b of the Pd $3d_{5/2}$ line remained constant and equal to 335.3 eV up Nb coverage ~2.2 ML Nb and shifted by 0.5 eV upwards at the highest Nb loading (Fig. 4). Very small changes of the width (W) of the Pd 3d line were observed after Nb deposition. The W of Pd $3d_{5/2}$ of clean Pd was 2.05 eV. The line becomes slightly broadener after deposition of Nb up ~4.7 ML Nb (W = 2.15 eV).

TABLE I

Binding energies E_b (eV) of the Nb $3d_{5/2}$ (Pd $3d_{5/2}$) photoelectron lines of Nb/Pd and Pd/Nb bimetallic systems, E_b shifts (ΔE_b (eV)) of the Nb $3d_{5/2}$ photoelectron line (relative to the E_b of metallic Nb), and relative intensities the high energy Pd 3d satellite I^{sat} of Nb/Pd system

Sample	E_b (Nb $3d_{5/2}$)	ΔE_b	E_b (Pd $3d_{5/2}$)	I^{sat}
0.1 ML Nb/Pd	204.3	2.1	335.3	0.86
1.2 ML Nb/Pd	204.0 ± 0.1	1.8	335.3	0.79
4.7 ML Nb/Pd	203.45	1.25	335.7	0.18 ± 0.10
0.8–5.4 ML Pd/Nb	202.2 ± 0.1 203.5 ± 0.2	1.30	335.6[a] 335.2[b]	

[a] 0.8 ML Pd. [b] 4.4 and 5.4 ML Pd.

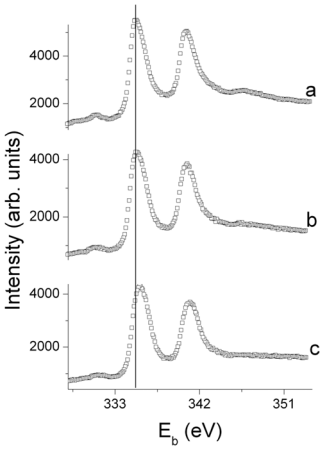

FIG. 4

The Pd 3d spectra of clean palladium support (a), and after Nb deposition 1.2 ML Nb (b) and 4.7 ML Nb (c)

The intensity of the high energy Pd 3d satellite decreased with increasing amount of the Nb deposited. The fitting procedure employed did not allow for an accurate determination of rather low intensity satellites. Consequently, the intensities of these satellites are discussed only qualitatively in this contribution. The spectra were normalized to unit height after inelastic background subtraction. The E_b(Pd $3d_{5/2}$) values of the spectra were zeroed to maximize the overlap. The evaluated high energy Pd 3d satellites of the samples with increasing Nb loading are depicted in Fig. 5a. The heights of the Pd 3d satellites are plotted as a function of Nb loading and are summarized in Fig. 6. The intensity of the Pd 3d high energy satellite also decreased in the Pd/Nb system with decreasing Pd loading (Fig. 5b). The satellite intensity decrease was accompanied by an increase in its separation from the main Pd 3d line in this system.

The kinetic energy E_k of electrons emitted by the Pd $M_5N_{4,5}N_{4,5}$ ($^1G_4$) Auger transition decreased with increasing Nb loading (E_k = 327.7 eV for clean Pd, 326.45 ± 0.3 eV for Pd with Nb loading ≥2.2 ML Nb (Fig. 7).

The binding energies of the Nb $3d_{5/2}$ and Pd $3d_{5/2}$ photoelectron lines, the binding energy shifts of the Nb $3d_{5/2}$ photoelectron line relative to its

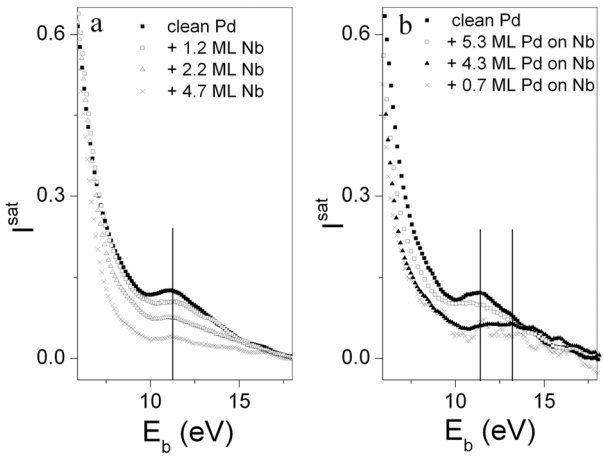

FIG. 5
The high energy Pd 3d satellites of the samples with increasing Nb loadings on Pd support (a) and Pd loadings on Nb support (b). The results for a sample prepared by evaporation of 4.3 ML Pd on the Nb surface is adopted from ref.[4]

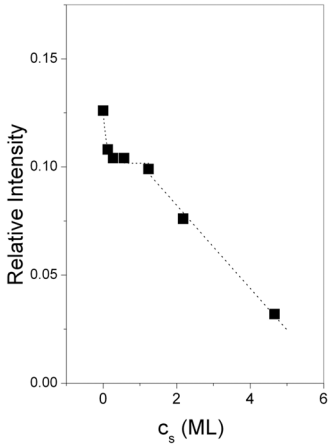

FIG. 6
Intensity of the high energy Pd 3d satellite I^{sat} in dependence on the surface concentration c_s (ML Nb) of Nb

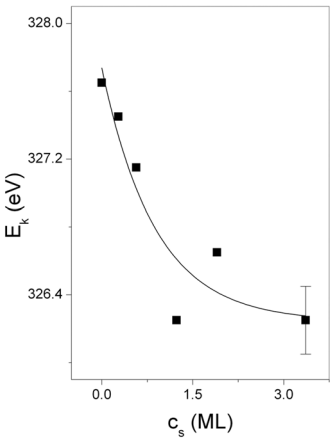

FIG. 7
Dependence of the kinetic energy E_k (eV) of the Pd $M_5N_{4,5}N_{4,5}$ Auger electrons on the surface concentration c_s (ML Nb) of Nb

value in pure Nb and the heights of the high energy Pd 3d satellite (I^{sat}) are summarized for selected Nb loadings in Table I. The heights are normalized relative to the value in clean Pd metal.

DISCUSSION

The dependence of the intensities of the Nb 3d photoelectron spectra on deposition time t (Fig. 1) is in the region of low Nb coverages ($t \leq 240$ s) typical for 2D growth mode of the Nb deposits on Pd. The change in the slope of this dependence in the Nb 3d spectra at 240 s can be explained as due to completion of the first Nb monolayer. The calculated value of the Nb surface concentration c_s at this time is equal 1.2 ML Nb, i.e. the error of estimation of Nb surface concentration is ~20%. This finding is in line with the fact that strong bimetallic bonding generally occurs between metals with low and high occupancy of d electron band[5,6]. This effect was well documented for the metal–metal interaction of vanadium adatoms on the surface of Pd(111) [16,17]. As V precedes Nb in the Vb group of the Periodic Table, analogous results may be expected also for the Nb–Pd surface bonding. Only fraction of V atoms remained on the Pd(111) surface after their adsorption already at room temperature in the region of submonolayer V coverage. The strong V–Pd attraction accompanied simultaneously with V–V adatom repulsion on a Pd(111) surface (S) induces exchange of surface Pd atoms by V atoms. A part of V atoms thus forms the V–Pd alloy in S-1 subsurface layer. The alloy formation is proposed to start at defect sites and step edges. Further dilution of the V atoms into deeper palladium subsurface region is energetically less favorable than their localization in the S-1 layer. These findings follow from investigation of the V/Pd(111) system by means of scanning tunneling microscopy, low energy ion scattering and Auger electron spectroscopy and are further supported by *ab initio* calculations of the energetics of V–Pd interaction[16,17].

The fact that the Nb deposits on polycrystalline Pd surface behave in an analogous manner is supported by the observation that the Pd 3d intensity is independent of the time of Nb deposition up t = 240 s, where a monolayer of Nb is deposited. This effect indicates dilution of Nb in the surface region of Pd. For a compact Nb monolayer on Pd the Pd 3d intensity would be attenuated by ~15% (see Fig. 1). Thus the Nb–Pd intermixing in the Nb-submonolayer region occurs similarly as in the V/Pd system. However, the effect of this shallow diffusion of Nb adatoms on the calculated Nb concentration is due to the high values of inelastic mean free paths λ of the photo-

electrons emitted from Pd 3d and Nb 3d levels within an experimental error of estimation of c_s.

Comparing the behavior of Nb/Pd system with that of V/Pd in the region above one monolayer is impossible because the V/Pd system has not yet been investigated in that concentration region. However, as follows from the explanation of the further effects appearing in the Nb 3d photoelectron spectra, and in the Pd 3d photoelectron spectra together with Auger Pd $M_5N_{4,5}N_{4,5}$ spectra (see below), substantial Nb–Pd intermixing occurs at room temperature above a monolayer coverage of Nb.

Nb 3d Photoelectron Spectra

The binding energies and line-shapes of the Nb 3d spectra, summarized in Fig. 2, reflect the absence of a distinct Nb phase throughout the investigated concentration region of Nb. In the case of layer-by-layer growth mode of Nb deposits on the Pd surface above the monolayer coverage the sample would contain also Nb atoms that are not directly bonded to Pd. This effect would likely result in the appearance of a new Nb 3d line with an E_b lower than the value corresponding to Nb atoms bonded to Pd. The intensity of this line would be comparable to or greater than intensity of the line assigned to the Pd–Nb bimetallic system depending on the surface coverage of Nb. However, only subtle changes were observed in the line shape of the Nb 3d spectrum with increasing Nb loading (see Figs 2 and 3b). No low-energy line was observed in the Nb 3d spectrum. Therefore, most of the evaporated Nb atoms are still coordinated to Pd even at the highest Nb loading.

Two doublets were observed in the Nb 3d photoelectron spectrum in the Pd/Nb system. The low energy Nb $3d_{5/2}$ line at E_b = 202.2 eV belongs to Nb metallic atoms of the substrate. The E_b(Nb $3d_{5/2}$) of the high energy Nb $3d_{5/2}$ line has been assigned to the Nb atoms bonded to Pd (203.5 eV)[4]. The E_b(Nb $3d_{5/2}$) of the thick adlayer on Pd (4.7 ML Nb) is the same within experimental error, as the high energy E_b(Nb $3d_{5/2}$) line of Pd/Nb system (see Table I). The values of these shifts are within the range of the shifts of E_b of Nb $3d_{5/2}$ line (1.1–1.6 eV) calculated for Nb–Pd bulk alloy[8]. This indicates that extensive mixing of the Pd and Nb atoms in the Nb/Pd system at highest Nb coverage has taken place at room temperature.

Pd 3d Photoelectron and Pd MNN Auger Spectra

The binding energy of the Pd $3d_{5/2}$ line is shifted by +0.5 eV at the highest coverage of Nb. The width (W) of Pd $3d_{5/2}$ photoelectron spectrum increases only negligibly upon Nb deposition. The measured shift of Pd $3d_{5/2}$ binding energy is typical of Pd alloys with some electropositive metals[5,6]. Thus, Pd atoms bonded to Nb prevail in the measured region of the sample with the highest loading of Nb. In addition, the shift in the kinetic energy E_k of the Auger Pd $^1G_4$ $M_5N_{4,5}N_{4,5}$ line becomes evident with increasing amount of deposited Nb (Fig. 7). As the thickness of the surface layer sampled by Auger electrons is less than the thickness sampled by Pd electrons, the Auger spectra are more sensitive to changes occurring at the Nb–Pd interface. The invariance of the Auger E_k above a monolayer coverage of Nb and the absence of broadening of the Pd Auger line indicates that the sample region measured by Auger spectra in this Nb concentration region is quite homogeneous. The Nb adatoms and the Pd surface atoms thus mix in the samples with $c_s \geq 1$ ML Nb.

Both the intrinsic and the extrinsic losses affect the overall intensity of the high energy Pd 3d satellite. From a comparison of electron energy loss spectra (EELS) and photoelectron spectra of a series of Pd alloys[18] it can be concluded that intrinsic effects generally do not influence significantly the high energy Pd 3d satellite of Pd in its alloys. An extrinsic contribution was identified for clean Pd surface by EELS as a surface plasmon[19]. However, in the case of the series of Pd–V alloys the extrinsic loss spectrum does not have any pronounced influence on satellite position, shape or intensity[18]. A similar behavior may be expected for Pd–Nb alloys.

The intrinsic origin of the effects influencing the energy and the intensity of the Pd 3d satellite was also shown in the series of Pd–Cu alloys[7]. The intensity of the satellite decreased and its separation from the main line increased with increasing concentration of Cu in the alloy. Identification of the Pd 3d satellite final state was based on a comparison of its shift with that of the Auger Pd MNN line in the series of Pd–Cu alloys with increasing Cu concentration. These shifts were identical and higher than those of the main Pd 3d line. Qualitatively similar effects can be also observed in other Pd alloys with electropositive metals[5–8].

The intensity of Pd 3d lines belonging to the bimetallic form of Pd can be neglected in the Pd 3d spectrum at low concentrations of Nb (<1 ML Nb). On the other hand, the intensity of the Pd 3d satellite is already affected by very low concentrations of Nb ($c_s \sim 10^{-1}$ ML Nb after 30 s of Nb evaporation, see Fig. 6. We thus propose that the intensity changes in the Pd 3d

satellite in the submonolayer coverage by Nb are caused predominantly by extrinsic losses. They are manifested in disappearance of the Pd surface plasmon with increasing coverage of Nb. The intensity of the Pd surface plasmon decreases by ~20% upon deposition of Nb already at c_s ~ 0.1 ML Nb and then remains constant up to c_s ~ 1 ML Nb. The intrinsic effect cannot significantly affect the intensity of the Pd 3d satellite as only a small number of measured Pd atoms (less than ~10%) interact directly with Nb in the region of submonolayer coverage. A further substantial decrease in the satellite intensity (by ~80%) was observed above c_s ~ 1 ML Nb (Figs 4 and 5). This decrease is a consequence of intrinsic effects, i.e. a substantial number of detected Pd atoms are coordinated to Nb.

The aforementioned results further support above conclusions. The layer-by-layer growth mode does not take place for Nb deposits on polycrystalline Pd above 1 ML coverage. The Nb adatoms in concentration as high as ~4.7 ML Nb are quantitatively intermixed with Pd atoms of the support surface. This finding agrees with results of density functional calculations of the heat of segregation and of the surface mixing energy in the Nb–Pd bimetallic system[20]. A substantial intensity decrease of Pd 3d satellite can therefore be explained by intrinsic losses at high coverage of Nb. However, no correlation between the energy shift of the Pd 3d high energy satellite and the energy of Pd MNN Auger line, as was observed in the series of Pd–Cu alloys[7], takes place in the Nb–Pd system. While a decrease in E_k of the Auger Pd $^1G_4$ $M_5N_{4,5}N_{4,5}$ transition with increasing c_s is evident in Fig. 7, no shift in the energy of the high Pd 3d satellite is discernible (Fig. 5a). This finding can be explained by an oversimplification in the evaluation of the position of the high energy Pd 3d satellite. The measured Pd 3d satellite is an envelope of the satellite lines belonging to the Pd atoms of the Pd metal and to bimetallic phase, respectively. Indeed, the decrease in intensity of the high energy Pd 3d satellite observed in an inverse experiment for the Pd–Nb system is accompanied by an increase in its separation from the main line (Fig. 5b). The number of Pd atoms bonded to Nb is sufficiently high in the Pd/Nb system to influence the position of the Pd 3d satellite.

CONCLUSIONS

The 2D-like growth mode of Nb–Pd surface alloy phase at room temperature on the polycrystalline surface of Pd has been demonstrated for submonolayer coverages of Nb. This growth mode is similar as observed by others for Pd adatoms on Nb monocrystalline surfaces[9,10]. Further 3D alloying of the Nb deposits with the atoms of Pd support proceeds at room tem-

perature above a monolayer coverage of Nb. All Nb adatoms are alloyed up 4.7 ML Nb, i.e. no evidence is found for the presence of distinct Nb phase on Pd support in this concentration region. According discussion of the energies and shapes of photoelectron Nb 3d and Auger Pd MNN lines is the Nb–Pd alloy phase rather homogeneous. However, some heterogeneity of Nb–Pd interface was found by discussion of the chemical effects of the high energy Pd 3d satellite.

This work was supported by Grant No. IAA400400625 of the Czech Science Foundation.

REFERENCES

1. Paglieri S. N., Way J. D.: *Sep. Purif. Methods* **2002**, *31*, 1.
2. Armor J. N.: *Catal. Today* **1995**, *25*, 199.
3. Jantsch U., Manhardt H., Lupton D. F.: U.S. 6800392, 2004.
4. Jirka I., Bastl Z.: *Czech J. Phys.* **2003**, *53*, 11.
5. Rodriguez J. A.: *Surf. Sci. Rep.* **1996**, *24*, 225.
6. Rodriguez J. A.: *Heterogen. Chem. Rev.* **1996**, *3*, 17.
7. Martensson N., Nyholm R., Johansson B.: *Phys. Rev. Lett.* **1980**, *45*, 754.
8. Weinert M., Watson R. E.: *Phys. Rev. B* **1995**, *51*, 17168.
9. Ciszewski A., Brona J., Zuber S. M., Szczudlo Z., Losovoy Ya. B.: *Prog. Surf. Sci.* **2003**, *74*, 25.
10. Brona J., Ciszewski A.: *Appl. Surf. Sci.* **2004**, *222*, 432.
11. Briggs D., Seah M. P. (Eds): *Practical Surface Analysis by Auger and X-ray Photoelectron Spectroscopy*. John Wiley, New York 1983.
12. Tanuma S., Powell C. J., Penn D. R.: *Surf. Interface Anal.* **1991**, *17*, 911.
13. Scofield J.: *J. Electron Spectrosc. Relat. Phenom.* **1976**, *8*, 129.
14. Weast R. C. (Ed.): *Handbook of Chemistry and Physics*. CRC Press, Cleveland, Ohio 1976.
15. NIST Standard Reference Database 20, version 3.4; http://www.
16. Konvicka Ch., Jeanvoine Y., Lundgren E., Kresse G., Schmid M., Hafner J., Varga P.: *Surf. Sci.* **2000**, *463*, 199.
17. Hirschl R., Hafner J.: *Surf. Sci.* **2002**, *498*, 21.
18. Hilebrecht F. U., Fuggle J. C., Bennett P. A., Zolnierek Z.: *Phys. Rev. B* **1983**, *27*, 2179.
19. Hagelin H. A. E., Weaver J. F., Hoflund G. B., Salaita G. N.: *J. Electron Spectrosc. Relat. Phenom.* **2002**, *124*, 1.
20. Christensen A., Ruban A. V., Stoltze P., Jacobsen K. W., Skriver H. L., Norskov J. K., Besenbacher F.: *Phys. Rev. B* **1997**, *56*, 5822.